Exp Fluids (2009) 46:631–641
DOI 10.1007/s00348-008-0588-z

RESEARCH ARTICLE

2-D PIV measurements of oscillatory flow around parallel plates

P. C. H. Aben · P. R. Bloemen · J. C. H. Zeegers

Received: 2 November 2007 / Revised: 9 October 2008 / Accepted: 21 October 2008 / Published online: 14 November 2008

Abstract Oscillatory flow in stacks of parallel plates is essential for the working of "standing wave" thermoacoustic devices. In this paper, the flow in the transition from stack to open tube is studied experimentally using particle image velocimetry. When the flow is directed outwards of the stack, vortices originate behind the stack plates. The Strouhal to Reynolds ratio determines the vortex pattern behind the stack plates, varying from a single vortex pair to a complete vortex street. The influence of different plate-end shapes and porosities are also studied. The streaming velocity is measured using two different methods.

1 Introduction

A vast amount of research in the field of thermoacoustics has been conducted in the last decades (Garrett 2004). Rott (1969, 1973, 1974, 1975, 1980), Rott and Zouzoulas (1976) and Swift (1988, 2002) have derived analytical equations describing thermoacoustics. This linear theory, however, is only valid at a relatively small drive ratio, which is defined as the pressure amplitude to average pressure ratio. The linear theory is in good agreement with measurement for drive ratios smaller than 10% (Swift 1995). The theory is used as basis for designing thermoacoustic applications. In many applications, however, large drive ratios (more than 10%) are used. At larger drive ratios, unfortunately, the coefficient of performance (COP), which is defined as the cooling power to work ratio, is strongly decreased. This might be attributed to nonlinear effects occurring at these high drive ratios, like turbulence, vortex formation, streaming, and higher harmonics. The study of nonlinear effects has become an important issue in thermoacoustics. This paper focusses on the vortex formation at the end of a parallel-plate stack.

Steady flow around obstacles, especially circular cylinders, is well-known (Kundu and Cohen 2004). In case of $Re < 1$ (the Reynolds number is defined here as $Re = \frac{V_\infty D}{\nu}$, with V_∞ the velocity far away from the cylinder, D the cylinder diameter, and ν the kinematic viscosity) the Stokes approximation can be used. The vorticity, which is created close to the cylinder surface due to the no-slip boundary condition, is not advected, resulting in a symmetrical flow. At increasing Reynolds numbers twin vortices appear ($4 < Re < 40$), a vortex street develops ($40 < Re < 200$), that finally becomes unstable ($Re > 200$), and even turbulent ($Re > 5{,}000$).

Oscillatory flows around single circular cylinders have been studied recently by Nehari et al. (2004), Anagnostopoulo and Minear (2004), Wybrow et al. (1996), and others. Parallel plates have a rectangular shape instead of circular. Ozgoren (2006) studied the flow structure behind both square and circular cylinders using DPIV. A stack of parallel plates is much different from a single circular cylinder. Not much is known about oscillatory flow around rectangular cylinders and certainly not about oscillatory flow around a stack of parallel plates. Since the length of the plates (130 mm) is much larger than the acoustic displacement (<7 mm), the two stack edges can be studied separately. A stack edge can be modeled as an oscillating flow through an array of channels into a volume. This geometry is very similar to a channel with a sudden change in cross-section. Oscillating flow in channels with a sudden

P. C. H. Aben (✉) · P. R. Bloemen · J. C. H. Zeegers
Department of Applied Physics,
Eindhoven University of Technology, Den Dolech 2,
Eindhoven, The Netherlands
e-mail: p.c.h.aben@tue.nl

change in cross-section have been studied by Ibrahim and Hashim (1994), and Morris et al. (2004) numerically and by Smith (2004), Smith and Swift (2003), and Skulina (2005, 2006) experimentally, using PIV and microphone measurements. Oscillatory flow through a rapid expansion was also studied by Smith and King (2007), and Smith et al. (2005). This is a similar geometry as a jet pump, which was studied by Petculescu and Wilen (2003).

Not much research has been conducted on the flow around a stack of parallel plates specifically. Stoltenkamp (2007) studied steady flow around stacked plates at an angle concerning a rotor. Oscillating flow around stacked plates has been studied experimentally using PIV and also numerically by Blanc-Benon et al. (2003) at relatively low amplitudes, where a vortex pair originates behind the stack plates and no vortex streets appear. Berson et al. (2006, 2008), Berson and Blanc-Benon (2007) and Mao et al. (2007) recently have measured a vortex street behind parallel plates at higher amplitudes using PIV. The interaction of the flow with that of a stack and heat exchangers is studied numerically by Besnoin and Knio (2004). The heat exchange, velocity field, vorticity and temperature distribution at the end of a stack are calculated. However, until now, no systematic experimental research has been undertaken on the flow patterns behind stack plate, in which all the relevant parameters (plate thickness and separation, velocity amplitude, frequency, and plate-end shape) are varied and their influence on the flow structure is studied.

This paper focusses on oscillatory flow through a stack. The vortex formation as well as streaming at the end of a parallel plate stack is studied using PIV. Vortex formation not only leads to dissipation, but can also influence the efficiency of the heat exchanger. Streaming can create an unwanted enthalpy flow in a stack or a regenerator. In Sect. 2, relevant parameters are defined. In Sect. 3, the experimental set-up is described and in Sects. 4 and 5, the experimental results of the vortex formation measurements and the streaming measurements, respectively, are presented.

2 Dimensionless numbers

It is convenient to describe our problem with dimensionless parameters. In this way, results of experiments or studies can be compared to similar situations. It also reduces the amount of data required to completely describe a problem.

2.1 Oscillatory 2-D flow between two infinitely long parallel plates

In case of an incompressible oscillatory flow in between two infinitely long parallel plates (Fig. 1), the angular

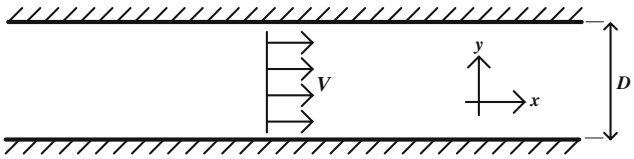

Fig. 1 A 2-D geometry consisting of a fluid oscillating at a cross-sectional average velocity $V(t)$ between two parallel plates at a distance D

frequency ω, cross-sectional average velocity amplitude V ($\widetilde{V}(t) = V\cos(\omega t)$), kinematic viscosity ν and plate separation D describe the problem, only two dimensionless parameters are relevant. The Reynolds number ($Re = \frac{VD}{\nu}$) and Strouhal number ($St = \frac{fD}{V}$) suffice, but often the Womersley number ($Wo = \sqrt{St\,Re}$) is more convenient than the Strouhal number. The Reynolds number determines whether the flow is turbulent, laminar or in transition. The Womersley number is the ratio between the plate separation and the viscous penetration depth ($\delta_\nu = \sqrt{\frac{2\nu}{\omega}}$). Let us consider a laminar flow. For low Wo number the viscous term is dominating the instationary term and the velocity has a Poiseuille profile, which is similar to a developed stationary flow. For high Wo number the flow only experiences the influence of one of the plates. The velocity parallel to the plates is given by Swift (2002)

$$u(y,t) = \mathcal{R}\left\{\frac{\mathrm{i}}{\omega\rho_\mathrm{m}}\left(1 - \frac{\cosh[(1+\mathrm{i})y/\delta_\nu]}{\cosh[(1+\mathrm{i})D/2\delta_\nu]}\right)\frac{\mathrm{d}p}{\mathrm{d}x}\mathrm{e}^{\mathrm{i}\omega t}\right\}, \quad (1)$$

with $y = 0$ in the center of the channel, ρ_m the mean density and $\mathcal{R}\{x\}$ representing the real part of x. At higher Re or higher Wo the flow becomes turbulent (Swift 2002). The transition occurs at a critical Reynolds number based on the viscous penetration depth: $\frac{Re_{\delta,c}}{\sqrt{2}} = \frac{V}{\sqrt{\nu\omega}} \approx 400$ (Merkli and Thomann 1975).

2.2 Oscillating 2-D flow in interaction with a finite length parallel plate stack

When a stack as part of a tube is considered (Fig. 2), two other parameters come into play: the porosity $D/(D + d)$ and the stack length L. The stack length can be included using the Keulegan-Carpenter number ($KC = \frac{V}{\omega L}$), which is the ratio of the displacement amplitude V/ω and the stack

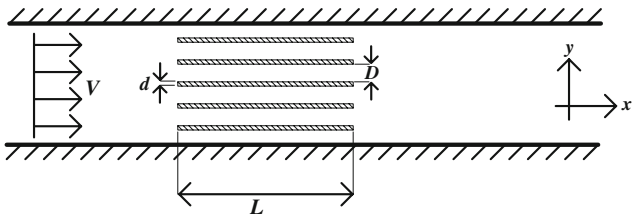

Fig. 2 A parallel plate stack of length L, plate thickness d and plate distance D inserted into a channel

length L. For a finite length stack the end effects become also important. For our experiments, it is advantageous to use relatively low frequencies (125 Hz). The Womersley number is frequency dependent. When decreasing the frequency and keeping the Womersley number constant, the plate spacing increases according to

$$D \sim \frac{1}{\sqrt{\omega}}. \tag{2}$$

3 Experimental set-up

The measurements are performed in a loudspeaker-driven standing-wave set-up. The set-up consists of a cylindrical perspex resonance tube, with an inner diameter of 25 mm and a total length of 1,400 mm (Fig. 3). The tube is closed with a transparent endplate on the left end, connected to a Dynaudio D54AF loudspeaker on the right end, and is filled with atmospheric air at room temperature. The first resonance frequency in our setup occurs at 125 Hz. At different locations microphones are inserted in the tube wall for measuring the pressure. A stack of parallel plates is placed 350 mm in front of the endplate. The flow-field measurements occur at the left end of the stack. A close-up of this measurement area is shown at the bottom of the figure. At the field of view the tube has a smaller wall thickness to increase its optical transparency. The observation window is still thick enough not to act as a membrane and start vibrating. The field of view is in the center of the tube and perpendicular to the stack plates.

For visualizing the velocity field between and behind the stack plates particle image velocimetry (PIV) is used. All measurements are made with a 15 Hz PIV system from LAVISION. For illumination a New Wave ND-YAG laser is used, which produces 2 × 50 mJ with a pulse length of

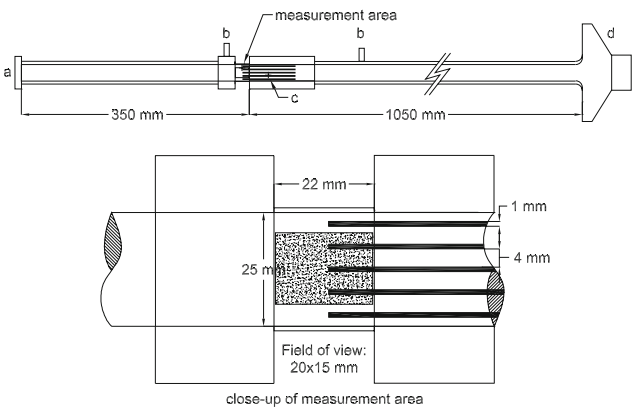

Fig. 3 Schematic drawing of the experimental set-up. At the *top* a resonance tube connected to a loudspeaker. **a** Transparent endplate, **b** injection nozzles for seeding, **c** stack of parallel plates, **d** loudspeaker. At the *bottom* a close-up of the measurement area

5 ns. Laser sheet optics in front of the laser create a laser sheet that coincides with the measurement area and has a thickness of 0.5 mm. Images are recorded with a 1,600 × 1,200 pixels^2 Imager Pro camera. Diethyl hexyl sebacate (DEHS) seeding particles are created by a Palas AGF2.0 seeding generator. The mean particle size, distributed by the seeding generater, is 200 nm, with a maximum particle size of 1 μm.

An airflow through the resonance tube is generated during the preparation of each measurement, to create a homogeneous aerosol distribution over the measuring volume. The particles are injected through a nozzle in front and released through a nozzle behind the measurement section. After closing the nozzles, the seeding density in the measurement section is sufficiently high. After the injection nozzles are closed, the injection flow has to be decayed sufficiently, before measurements can be performed. This is important for streaming measurements in particular. From test measurements it was concluded that 1 min after closing the injection nozzles, no significant flow (smaller than 0.2 mm s^{-1}) was present in the measurement area. The effect of the seeding particles on the speed of sound, determined by measuring the resonance frequency, is found not to be significant. The presence of the particles leads to an increase of the speed of sound by 0.5%.

In most thermodynamic devices, in general, a frequency of the order 0.1–1 kHz is used. In our experiments, we have chosen to use a low frequency: 125 Hz (only in Sect. 4.3, to study the frequency dependency, additional measurements at the second and third resonance frequencies, 240 and 372 Hz, are performed). This has two advantages for visualization:

1. the required time resolution of the laser and camera is lower;
2. the plate separation of the stack can be larger as a consequence of larger penetration depths.

The latter follows from Eq. 2. The stacks that are used consist of 5 parallel perspex plates. The plate thickness d is in most measurements 1 mm and the plate distance D = 4 mm. To study the influence of the plate thickness in some measurements, stacks with a plate thickness of 0.5 mm and a plate distance of 4.5 mm are used, as well as single plates with a thickness of 3 mm. The stack length is 130 mm. To reduce laser light reflections all stack plates are coated black.

4 Vortex shedding results

At the end of a stack the open cross-section suddenly changes. This sudden area change causes some interesting

flow effects like vortex formation and jet streaming. In this section, we will only discuss the vortex shedding. The streaming is discussed in the next section.

4.1 A typical measurement

The vortex formation is studied using PIV at the left side end of a stack. In this typical measurement the stack consists of five rectangular plates with the following geometry parameters: $d = 1.0$ mm, $D = 4.0$ mm and $L = 130$ mm. The Reynolds and Strouhal numbers are here defined as:

$$Re = \frac{Vd}{v}, St = \frac{fd}{V}, \tag{3}$$

with V the peak velocity of the main flow just outside the stack. The peak velocity inside the stack is higher than V due to a smaller gas area inside the stack. The flow can be characterized by $f = 125$ Hz, $p = 3.7$ kPa, $V = 5$ m s^{-1}. This corresponds to $Re = 3.3 \times 10^2$ and $St = 2.5 \times 10^{-2}$. The viscous penetration depth, $\delta_v = 0.2$ mm. The phase angle at which the measurement has been performed, $t_0\omega = \pi$. This is the moment at which the main flow is at rest and the particles are at their leftmost excursion. During the measurement one picture is taken at $t_1 = t_0 - \Delta t/2$ and a second at $t_2 = t_0 + \Delta t/2$. The time between the pictures, Δt, is chosen such that the maximum particle displacement is roughly 5 pixels, which is 1/6 of the size of an interrogation window (Raffel et al. 1998). By a cross-correlation algorithm the two pictures are compared and the particle displacement at different positions is determined. The particle displacement is divided by the time difference Δt, resulting in a velocity field that is shown in Fig. 4a. The vector lengths (in the top left corner of the picture) and colors (Fig. 5a) are a measure for the magnitude of the velocity vectors. The black rectangles represent a part of the stack plates. In total 100×75 vectors are determined, which corresponds to a resolution of 14 vectors mm^{-2}. However, to keep the individual vectors visible, the resolution of the images in this paper are lower. The relative error of the measured velocities is typically 1%.

When studying vortices originating at the the end of stack plates the vorticity,

$$\omega_z = \frac{\partial v}{\partial x} - \frac{\partial u}{\partial y}, \tag{4}$$

is a useful parameter. A vorticity plot of the same measurement is shown in Fig. 4b. The color bar in Fig. 5b shows the correspondence between color and vorticity. In this case $\omega_0 = 1.2 \times 10^4$ s^{-1}. At the end of each plate a street of alternating vortices is present. Remark that there is a slight phase shift between the forming of vortices behind the different plates (the red lines in Fig. 4b are not vertical). This could be caused by small disturbances in the inflow, especially for higher Reynolds numbers. However, an analysis of the flow, using PIV, showed that the wave is flat. Sufficiently far away from the stack (more than four times the particle displacement), the flow in the stack is symmetrical. The asymmetry of the flow patterns is probably caused by small asymmetries in the geometry.

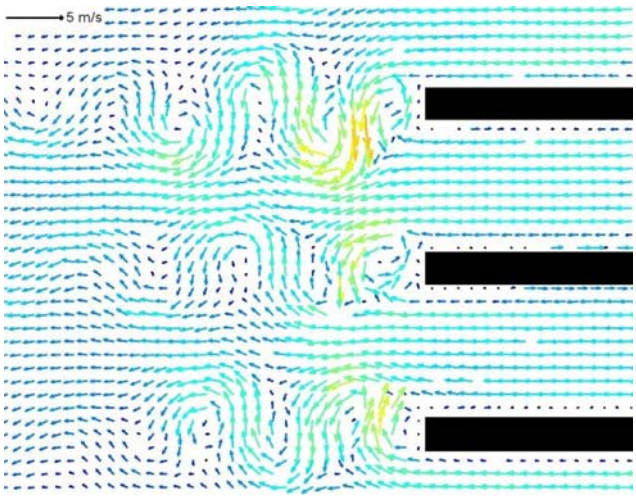

(a) velocity field

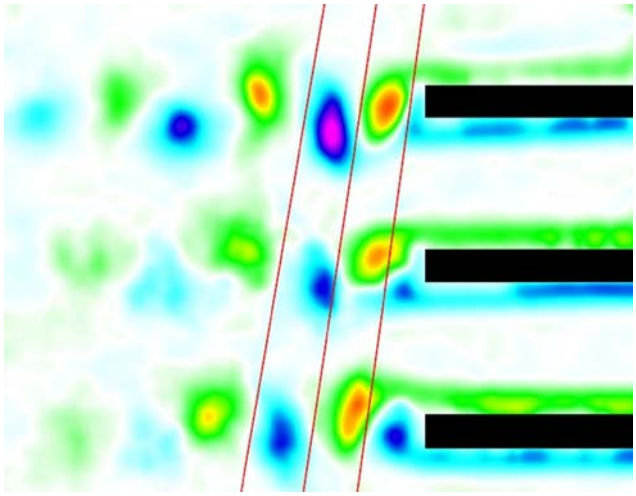

(b) vorticity plot

Fig. 4 A typical flow visualization measurement at the end of a stack. The *three black rectangles* represent (a part of) the stack plates, which are 1 mm thick and at a distance of 4 mm from each other. The frequency is 125 Hz and the velocity amplitude is 5.0 m s^{-1}

4.2 Vorticity as function of time

In Fig. 6f, the particle displacement of the main flow during one cycle is shown. The squares in this plot are moments during the cycle at which the measurement are performed. The vorticity at the end of a stack evolution is shown in Fig. 6a–e. The letters in Fig. 6f indicate which

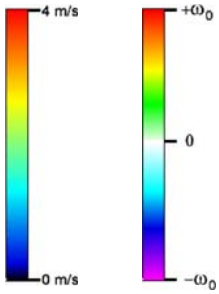

(a) velocity **(b)** vorticity

Fig. 5 *Color bars* that are used for coloring the velocity vectors and vorticity plots

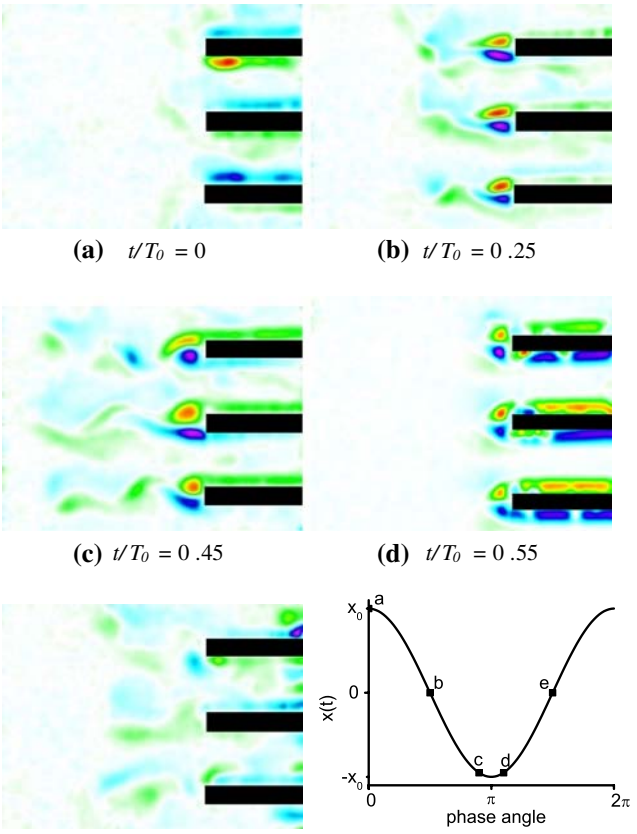

(a) $t/T_0 = 0$ **(b)** $t/T_0 = 0.25$

(c) $t/T_0 = 0.45$ **(d)** $t/T_0 = 0.55$

(e) $t/T_0 = 0.75$ **(f)** displacement as function of time during one cycle

Fig. 6 Vorticity plots during one cycle. The *three black rectangles* represent (a part of) the stack plates, which are 1 mm thick and at a distance of 4 mm of each other. The frequency is 125 Hz and the velocity amplitude is 3.3 m s^{-1}. Figure 5 shows the *color bar* that is used ($\omega_0 = 1 \times 10^4$ s^{-1})

figure corresponds to which moment during the cycle. The Δt is adapted in each measurement in such a way that the displacement is roughly 5 pixels.

In Fig. 6a, the velocity of the main flow is zero and the particles are at the most rightward position. The strokes of positive vorticity beneath each plate and negative vorticity above each stack are the viscous boundary layers. When the flow is leftward (Fig. 6b) the vorticity in these boundary layers switches sign and at the end of each plate a vortex pair originates. Behind this vortex pair even more vortices are shed and a vortex street is formed (Fig. 6c, d). When the flow is rightward the vortices are convected inside the stack, where they become part of the viscous boundary layers (Fig. 6e).

4.3 Amplitude dependence

We consider the vorticity at the moment in a cycle at which the velocity of the main flow is zero and the particles are at their leftmost excursion. The frequency and geometry for each measurement are kept the same and the velocity amplitude of the main flow is increased. The vorticity plots for four different velocity amplitudes are shown in Fig. 7.

Figure 8 is a simplified drawing of the different vortex patterns that occur at the end of a plate when the amplitude is increased. We can divide the vorticity plots at the stack end into four categories:

(A) *two vortices* Two vortices of opposite sign (a dipole) are formed behind each stack plate, as is shown in Figs. 7a and 8a.

(B) *four vortices* Behind each stack plate four vortices are formed, as is shown in Figs. 7b and 8b.

(C) *transition area* A category in between four vortices and a vortex street, as is shown in Fig. 7c. The distinction between this category and categories B and C is somewhat arbitrary. A vortex pattern is placed in

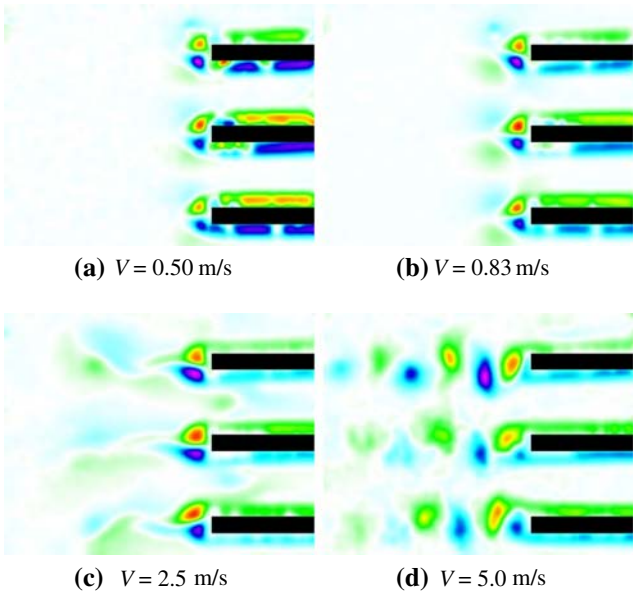

(a) $V = 0.50$ m/s **(b)** $V = 0.83$ m/s

(c) $V = 2.5$ m/s **(d)** $V = 5.0$ m/s

Fig. 7 Vorticity plots at the end of a stack at different velocity amplitudes. The *three black rectangles* represent (a part of) the stack plates, which are 1 mm thick and at a distance of 4 mm of each other. The frequency is 125 Hz

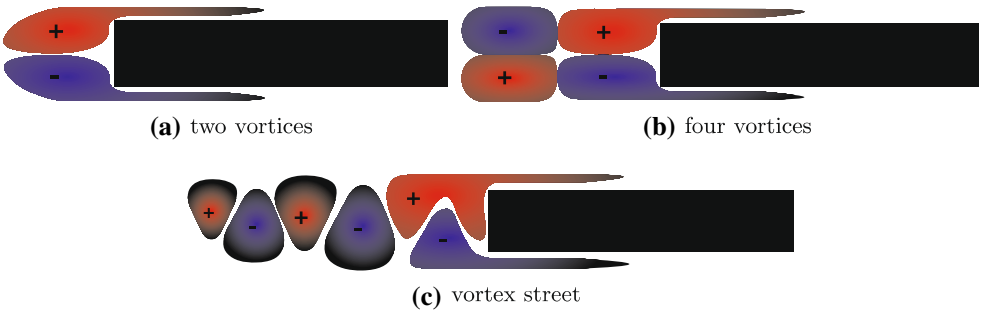

Fig. 8 Different categories of vortex formation at the end of a stack plate

category B when the number of vortices is four and the vortices are located directly behind the stack in a symmetrical way. In the transition area the number of vortices is larger than four or the vortices are not symmetrically located in the extension of the plate.

(D) *vortex street* A row of at least six vortices is formed behind each plate (Figs. 7d, 8c). A vortex pattern is called a vortex street when at least six vortices can be distinguished and the vortices are located in the extension of the plate.

The objective is to find a correlation between the category of vortex formation (A–D) and relevant dimensionless parameters (*Re* and *St*). At higher Reynolds numbers the instationary term of the Navier–Stokes equation becomes more important. Therefore we expect that at higher Reynolds numbers the flow is more inclined towards a vortex street than to two or four vortices. The Strouhal number is a ratio of the plate thickness and the displacement amplitude. The plate thickness is a measure for the vortex size in the direction perpendicular to the plate and the displacement amplitude determines the number of vortices in the direction parallel to the plate. The vortex size is based on the optical appearance in the vorticity plots. At low Strouhal numbers we expect the vortex to be more elongated and farther away from the plate and is therefore expected to be more inclined towards a vortex street.

In Fig. 9, the Strouhal number is plotted versus the Reynolds number for a set of 25 measurements with different frequencies (125, 240 and 372 Hz) and different velocity amplitudes (0.33 to 5.0 m s^{-1}). For each measurement the vorticity pattern is studied and is placed in one of the four categories. Depending on the category the data points in Fig. 9 have different symbols. There is a clear distinct correlation between the two relevant dimensionless parameters and the different categories. Each category has its own area in the Reynolds–Strouhal space. The two black lines indicate the boundaries between these areas. The lines can be described by the following function:

$$St/Re = fv/V^2 = \alpha, \tag{5}$$

in which α is a constant. For the border line between category B and D it follows that $\alpha = (10 \pm 2) \times 10^{-4}$ and for

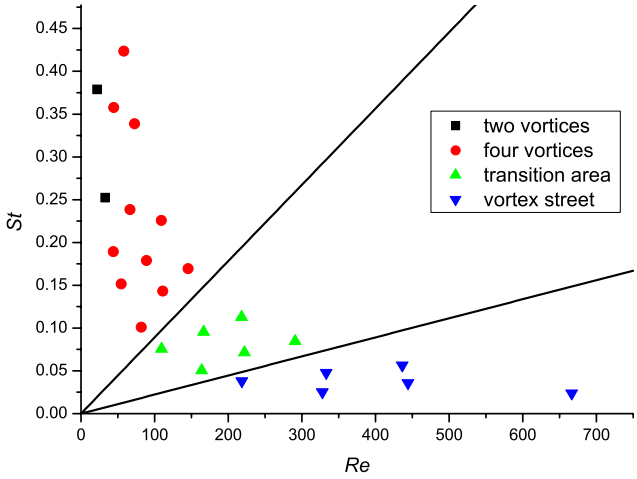

Fig. 9 The Strouhal number plotted versus the Reynolds number

the border line between D and C it follows that $\alpha = (2.3 \pm 0.5) \times 10^{-4}$. For the range of *Re* and *St* it seems that only the ratio *St*/*Re* is determinative for the category of vortex patterns occurring at the end of a plate.

$1/St$ is a measure for the number of vortices that can be formed. For $1/St \sim 2\pi$, i.e. $V/2\pi f \sim d$, only two vortices are expected, since the displacement length is approximately of the same size as the vortices. For a vortex street to be formed, two criteria need to be fulfilled:

(a) $1/St > 2\pi$, otherwise the displacement length is not long enough for more than two vortices to be formed,
(b) the *Re* number needs to be high enough for vortices to be formed.

4.4 Influence of plate thickness and spacing

So far, we only discussed the influence of the velocity and the frequency on the vortex patterns. Both *Re* and *St* also depend on the plate thickness *d*. The ratio of *St* and *Re*, on the contrary, does not depend on *d*. If our statement that the category of vortex patterns only depends on the ratio of *St* and *Re* is true, the plate thickness is expected to have no influence on the category of vortex patterns. To study this experimentally measurements were made with plate thickness of 0.5 and 1 mm.

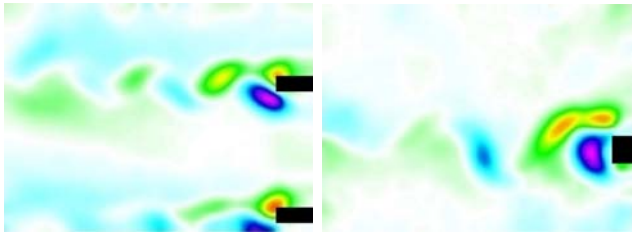

(a) Re=179, St=0.07, d=0.5 mm **(b)** Re=328, St=0.16, d=1.0 mm

Fig. 10 Vorticity plots for two different plate thicknesses at a porosity of 8/9 and at a frequency of 125 Hz

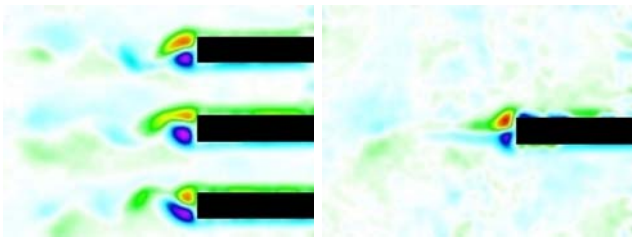

(a) 5 plates, d=1.0 mm, ϕ=0.80 **(b)** 1 plate, d=1.0 mm, ϕ=0.95

Fig. 11 Vorticity plots of five parallel plates and a single plate at a velocity of 3.3 m s^{-1} and a frequency of 125 Hz

The plate spacing is related to the plate thickness by a third dimensionless number, the porosity

$$\phi = \frac{D}{d+D}. \tag{6}$$

At a very high porosity ($\phi \rightarrow 1$) the stack can be modeled as a single plate with thickness d in an infinitely large 2-D medium. In this case the plate thickness is the relevant characteristic length. At a low porosity ($\phi \rightarrow 0$) the stack can be modeled as flow from a single 2-D opening with spacing D into an infinitely large medium. Now the spacing D is the relevant characteristic length.

We consider two geometries where $\phi = \frac{8}{9}$ in both cases (Fig. 10).

Since the amplitude and frequency are the same in both pictures, so is the stroke length V/ω. The vertical size of the vortices in Fig. 10b is roughly two times as large as in Fig. 10a. The vertical dimensions of the vortices are directly related to the plate thickness. The horizontal dimensions of the vortices are only slightly larger in Fig. 10b in comparison with Fig. 10b. The Reynolds number is in Fig. 10b two times as large as in Fig. 10a. In Fig. 11, we keep the plate thickness the same ($d = 1$ mm) but change the porosity. For lower porosities Fig. 11a the vortex patterns tends more toward a vortex street than Fig. 11b. There are several reasons for this. In Fig. 11a, the vortex pairs that originate behind each plate can influence each other. Also at lower porosities the change in velocity between the regions inside and outside the stack is higher.

In Fig. 12, we study three geometries with a single plate each time, with thickness $d = 0.5$, 1, and 3 mm, respectively. In Fig. 12c, the presence of a vortex street is not so obvious. The displacement amplitude V/ω is 6 mm, only two times as large as the plate thickness, and not large enough for a vortex street to be created. Due to this effect it seems reasonable that above a certain Strouhal number no vortex streets can be created.

4.5 Influence of plate end shape

So far all measurements were performed on rectangular plates with a flat end (Fig. 13a). In this subsection, we discuss the influence of the shape of the plate ends on the vortex shedding at the end of the plates. We measured the flow around single plates with a thickness of 3 mm. In Fig. 13b, the flow around a circular end is shown, in Fig. 13c around a 90° triangle and in Fig. 13d around a 25° triangle. Due to the absence of sharp corners for the circular end the vorticity plot is more smoothly and the two vortices are almost circles. The 90° triangle does have sharp corners and is very similar to a rectangular end. At the end of a 25° triangle however, two thin layers of vorticity are present behind the sharp corner. These two layers do not roll up. The vortex on top of the triangle is caused by the transition of a straight plate towards a triangle. The sharp triangular shape is clearly giving different results as the other geometries. The choice of a shape can influence the dissipation due to the vortices that are shed off and the heat

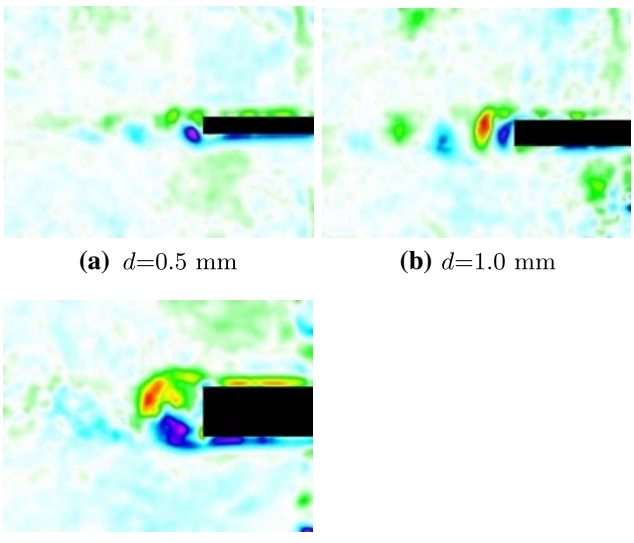

(a) d=0.5 mm **(b)** d=1.0 mm

(c) d=3.0 mm

Fig. 12 Single plates geometries with different plate thicknesses. The velocity amplitude of the main flow in all three pictures 5.0 m s^{-1} and the frequency 125 Hz

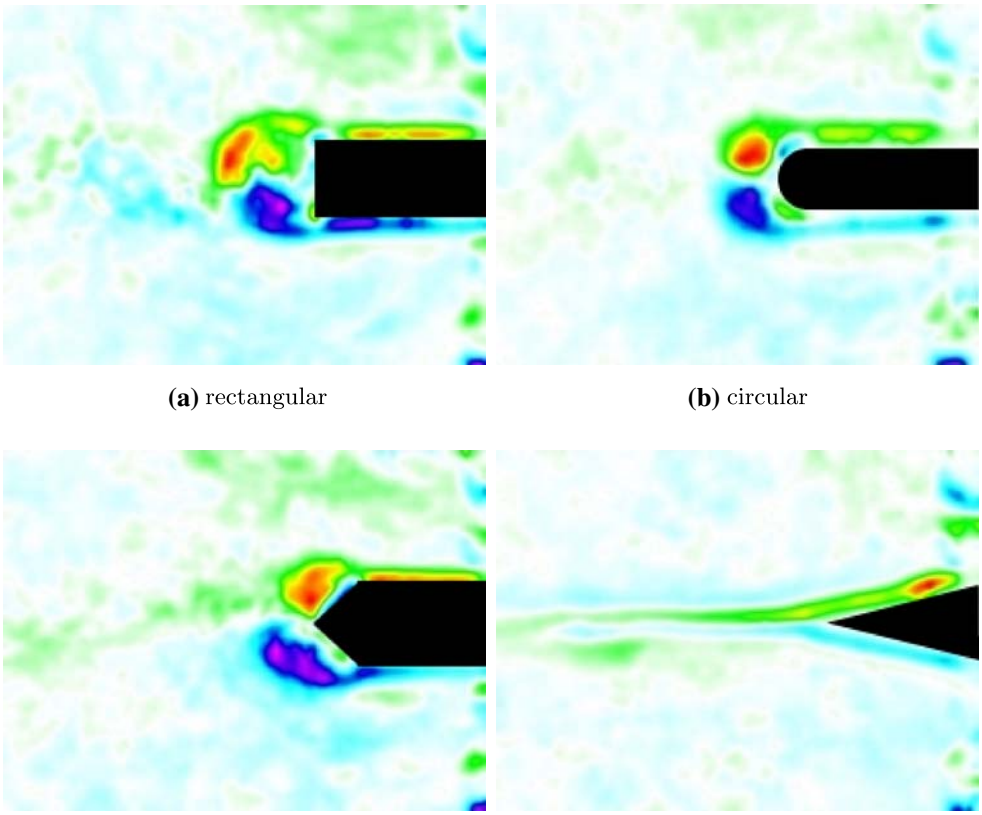

(a) rectangular **(b)** circular

(c) triangular **(d)** sharp triangular

Fig. 13 Vorticity plots of different plate ends. The plate thickness is 3.0 mm

transfer in the heat exchanger. At triangular ends with even sharper edges (12° or smaller) vortices completely disappear and the shear layer dissolves smoothly in the main stream.

5 Streaming results

When no streaming is present all seeding particles will return to their original positions after one cycle. If streaming occurs (Fig. 14) a netto displacement is generated. The streaming velocity is determined by dividing the netto displacement Δx by the time period Δt. Streaming effects can lead to a huge loss of efficiency in thermoacoustic devices due to convection (Swift 2002). We will discuss two different methods of measuring streaming by PIV: the phase method and the average method.

The streaming velocities are relatively small compared to the acoustic velocity amplitudes. It is therefore important that no background flow is present inside the tube before the measurement is started. The injection of seeding particles causes such a flow inside the tube, which can disturb our streaming measurements. From experiments it was concluded that 1 min after closing the injection

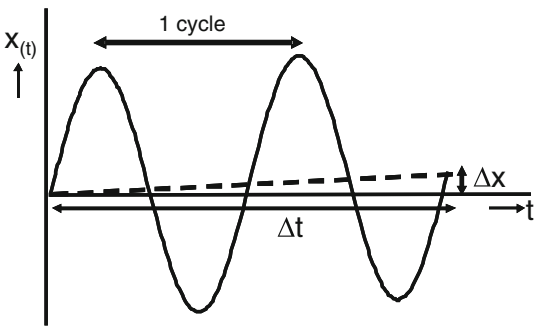

Fig. 14 Displacement of a particle as function of time

nozzles, the flow decayed sufficiently (smaller than 0.2 mm s^{-1}).

5.1 Phase method

For each PIV measurement an image pair is captured with a certain time interval Δt. When an instantaneous flow field is measured, Δt is optimized such that the ideal shift of particles is ensured (typically 5 pixels). The phase method to measure streaming is to take Δt equal to exactly one cycle period of the loudspeaker. When no streaming would be present all particles arrive in the same position as the

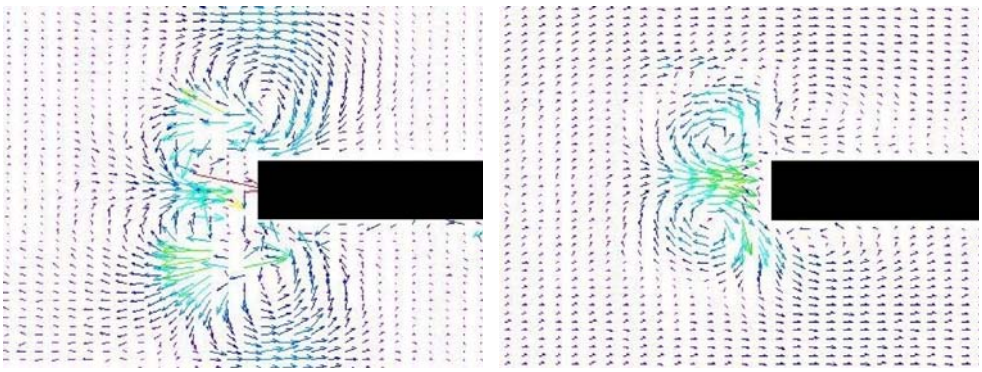

(a) Phase method **(b)** Average method

Fig. 15 Steaming velocity field measured with two different methods. The plate thickness is 1 mm, the plate separation 4 mm, the frequency 125 Hz and the velocity amplitude 0.3 m s^{-1}. The vector lengths and colors are normalized to the maximum value of the velocity in the figure

first image. Particles that experience streaming, have a small displacement with respect to their original position. The accuracy of this measurement method is expected to be comparable to normal PIV measurements, if timing is executed correctly, the particles stay in the light sheet and their movement during each cycle is reproducible. Though simple, this measurement technique also has some disadvantages:

(a) The freedom to optimize Δt such that the ideal particle shift is ensured is lost. Δt is now fixed to the cycle period of the system, and the user can only hope that the particle displacement is anywhere near optimal.
(b) Since Δt will be much higher now than for instantaneous measurement, clusters of seeding particles are more likely to change form, making it more difficult for the cross-correlation algorithm to find the right displacement.
(c) Also due to the higher Δt, particles are more likely to move out of the light sheet during a measurement.

These disadvantages make this technique only suited for low amplitude measurements. The most critical criterium is that the particles need to stay within the light sheet during a whole cycle. Small 3-D effects can make the method unusable.

This method is used to measure the streaming at the end of a stack of parallel plates (Fig. 15a) at a velocity amplitude of 0.3 m s^{-1}. At this amplitude it is not giving correct results. Since the tube is closed the cross-section integrated velocity should be zero everywhere, due to mass conservation. This is not true at the stack border. The measured streaming velocity between the plates is directed inwards the stack. The streaming velocity just in front of the stack plates is expected to be directed towards the plates, whereas the measured streaming velocity at this point is almost zero. The deviations are probably caused by particles moving out of the light sheet during the cycle.

5.2 Average method

A second way to generate a streaming vector field, is to split one cycle up into a large number of smaller periods. In each of these periods the instantaneous velocity field is measured using PIV. The streaming velocity field is determined by averaging the velocity fields of all different periods during one complete cycle.

An advantage of this method is that it is very flexible and both low and high amplitudes can be studied. A disadvantage of this method is that it can only be used when the flow is reproducible. Since this method is based on many separate measurements, the duration of one complete streaming vector field is roughly 3 s (with a 15Hz PIV system). The velocity needs to stay the same in every cycle during these 3 s.

Forty velocity fields are recorded at exactly 1/40 cycle time difference. All velocity fields are averaged and the resulting vector field gives streaming velocity as is shown in Fig. 15b. The measurement result of the streaming velocity field corresponds to what is expected. Two major velocity loops are created to the left of the plate. And two smaller loops are created just inside the stack: one on top and one below the plates. This measured streaming velocity

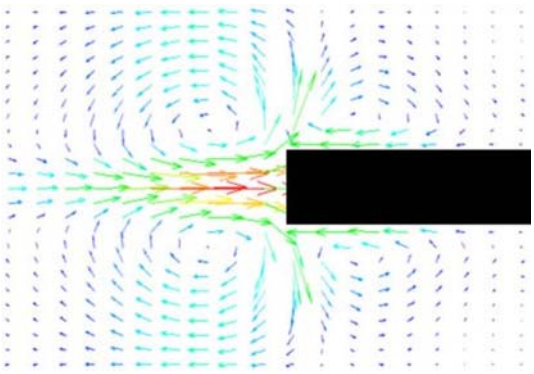

Fig. 16 Numerical CFD simulation of the streaming velocity field

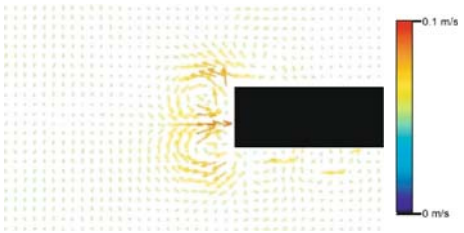

(a) velocity amplitude V = 0.5 m/s

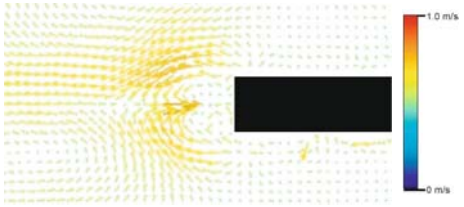

(b) velocity amplitude V = 2.5 m/s

Fig. 17 Streaming velocity field, measured with the average method, for two different velocity amplitudes. The vector lengths and colors are normalized to the maximum value of the velocity in the figure. The plate thickness is 1 mm, the plate separation 4 mm and the frequency 125 Hz

profile is qualitatively in agreement with a numerical CFD calculation that is shown in Fig. 16.

6 Results

The average method is used to determine the streaming velocity at two different velocity amplitudes as is shown in Fig. 17. Figure 17a is similar to Fig. 15b. The two major loops to the left of the plate can be clearly distinguished. The minor loops at the top and bottom of the plates are not so clearly visible, due to difficulties measuring very close to walls or plates. At higher amplitudes (Fig. 17b), to the left of the major vortex pair, two additional vortices are present. These two vortices have the opposite sign of the major vortex pair and have larger dimensions. These additional vortices are a result of a higher displacement amplitude as is explained in Sect. 4.3.

The root mean square (rms) value of a single measurement, using the phase method, is of the same order as the measured value of the streaming streaming velocity. The rms value of one series of 40 measurements, each at a different phase covering the whole cycle, using the average method, is roughly 20% of the measured streaming velocity.

7 Conclusions

The PIV has proven to be a useful measurement technique in the study of thermoacoustic flow around stacks of parallel plates. It is shown that different vortex patterns (one vortex pair, two vortex pairs, vortex street) can originate behind a parallel plate. The Reynolds and Strouhal numbers, and its ratio in particular, are the relevant dimensionless numbers for determining which vortex pattern occurs. The influence of porosity and plate end shape are also studied. The vorticity pattern behind sharp edged plate ends (25° or smaller) differs from squared or circular plate ends: instead of vortex pair or a vortex street two thin layers of vorticity are formed.

Two different streaming measurement methods, the phase method and the average method, are compared. In contrast to the phase method, the average method is giving good results.

Acknowledgments This research is financially supported by the Dutch Technology Foundation STW. The authors are also grateful for the discussions with A. Hirschberg and technical assistance provided by L. van Hout.

References

Anagnostopoulos P, Minear R (2004) Blockage effect of oscillatory flow past a fixed cylinder. Appl Ocean Res 26:147–153

Blanc-Benon Ph, Besnoin E, Knio O (2003) Experimental and computational visualization of the flow field in a thermoacoustic stack. C R Mecan 331:17–24

Berson A, Blanc-Benon Ph, Michard M (2006) Ecoulements secondaires aux extrémités du stack d'un réfrigérateur thermoacoustique: mesure des champs de vitesse oscillante àl'aide de la piv, in 8ème Congrès Français d'Acoustique, pp. 749–752

Berson A, Michard M, Blanc-Benon Ph (2008) Measurement of acoustic velocity in the stack of a thermoacoustic refrigerator using particle image velocimetry. Heat Mass Transfer 44:1015–1023

Berson A, Blanc-Benon Ph (2007) Nonperiodicity of the flow within the gap of a thermoacoustic couple at high amplitudes. J Acoust Soc Am 122(4):EL122–127

Besnoin E, Knio OM (2004) Numerical study of thermoacoustic heat exchangers. Acta Acust United Acust 90:432–444

Garrett SL (2004) Resource letter: Ta-1: thermoacoustic engines and refrigerators. Am J Phys 72:11–17

Ibrahim M, Hashim W (1994) Oscillating flow in channels with a sudden change in cross-section. Comput Fluids 23:211–224

Kundu P, Cohen I (2004) Fluid mechanics, 3rd edn. Academic Press, San Diego

Mao X, Marx D, Jaworski AJ (2007) Piv measurement of coherent structures and turbulence created by an oscillating flow at the end of a thermoacoustic stack, in Progress in Turbulence II Proceedings iTi Conference in Turbulence (M.Oberlack, ed.), vol.109, pp. 99–102

Merkli P, Thomann H (1975) Transition to turbulence in oscillating pipe-flow. J Fluid Mechan 68:567–575

Morris P, Boluriaan S, Shieh C (2004) Numerical simulation of minor losses due to a sudden contraction and expansion in high amplitude acoustic resonators. Acta Acust United Acust 90:393–409

Nehari D, Armenio V, Ballio F (2004) Three-dimensional analysis of the unidirectional oscillatory flow around a circular cylinder at low Keulegan-Carpenter and beta numbers. J Fluid Mechan 520:157–186

Ozgoren M (2006) Flow structure in the downstream of square and circular cylinders. Flow Meas Instrument 17:225–235

Petculescu A, Wilen LA (2003) Oscillatory flow in jet pumps: nonlinear effects and minor losses. J Acoust Soc Am 113(3):1282–92

Raffel M, Willert C, Kompenhans J (1998) Particle image velocimetry. A practical guide. Springer, Heidelberg

Rott N (1969) Damped and thermally driven acoustic oscillations in wide and narrow tubes. J Appl Math Phys 20:230–243

Rott N (1973) Thermally driven acoustic oscillations. Part II: stability limit for helium. J Appl Math Phys 24:54–72

Rott N (1980) Thermoacoustics. Adv Appl Mechan 20:135–175

Rott N (1974) The influence of heat conduction on acoustic streaming. J Appl Math Phys 25:417–421

Rott N (1975) Thermally driven acoustic oscillations. Part III: second-order heat flux. J Appl Math Phys 26:43–49

Rott N, Zouzoulas G (1976) Thermally driven acoustic oscillations. Part IV: tubes with variable cross-section. J Appl Math Phys 27:197–224

Smith BL (2004) Pressure recovery in a radiused sudden expansion. Exp Fluids 36(6):901–7

Smith BL, Swift GW (2003) Power dissipation and time-averaged pressure in oscillating flow through a sudden area change. J Acoust Soc Am 113(5):2455–63

Smith BL, King CV (2007) Time-resolved piv and pressure measurements of oscillating and pulsating flow in a rapid expansion, in 2007 5th Joint AMSE/JSME Fluids Engineering Conference

Smith BL, Mortensen KV, Wendel S (2005) Oscillating flow in adverse pressure gradients, in 2005 AMSE Fluids Engineering Summer Conference

Skulina D (2005) A study of non-linear flows at the open end of a tube using particle imaging velocimetry. PhD thesis, University of Edinburgh

Skulina D (2006) A study of non-linear acoustic flows at the open end of a tube using particle image velocimetry. J Acoust Soc Am 120(5):3363

Stoltenkamp P (2007) Dynamics of turbine flow meters. PhD thesis, Eindhoven University of Technology

Swift G (1988) Thermoacoustic engines. J Acoust Soc Am 84:1146–1180

Swift G (1995) Thermoacoustic engines and refrigerators. Phys Today, pp 22–28

Swift G (2002) Thermoacoustics: a unifying perspective for some engines and refrigerators. Acoustical Society of America

Wybrow MF, Yan B, Riley N (1996) Oscillatory flow over a circular cylinder close to a plane boundary. Fluid Dyn Res 18:269–288